JOURNAL OF GEOPHYSICAL RESEARCH, VOL. 96, NO. A8, PAGES 13,913–13,929, AUGUST 1, 1991

Plasma Waves Observed in the Near Vicinity of the Space Shuttle

IVER H. CAIRNS AND DONALD A. GURNETT

Department of Physics and Astronomy, University of Iowa, Iowa City

The OSS 1 and Spacelab 2 missions found intense broadband waves in the near vicinity of the space shuttle. This paper contains a detailed observational characterization and theoretical investigation of the plasma waves observed within about 10 m of the space shuttle during the XPOP roll period of the Spacelab 2 mission. High wave levels are found from 31 Hz to 10 kHz (near the lower hybrid frequency). Above 10 kHz the wave levels decrease with frequency, reaching the background level near 56 kHz. The frequency distribution of wave electric fields is best interpreted in terms of three components below about 10 kHz and a high-frequency tail. The primary component is a fairly uniform, high level of waves covering the frequency range from 31 Hz to 10 kHz. The two superposed components in this frequency range have electric fields of order twice the uniform level. The second component corresponds to a low-frequency peak in the range 100–178 Hz. The third component is found near, and follows the trend of, the lower hybrid frequency. No evidence is found for a high-frequency component localized above about 10 kHz. The waves show a pronounced amplitude and frequency variation with the quantity $V_\parallel/V_T$ which measures the angle between the ionospheric magnetic field and the shuttle's velocity vector. Very low wave levels and small frequency extents are observed when $V_\parallel/V_T \sim 1$ and the shuttle is moving primarily along the magnetic field. This implies that the waves are probably driven by water pickup ions. Observations of the waves below about 20 kHz during the free-flight mission imply that the near-zone waves have wave vectors oriented perpendicular to the magnetic field. The nulls observed in the wave data as the PDP spacecraft moves through the orbiter's wake imply that wavenumber increases with wave frequency. Hwang et al.'s theory for the near-zone waves is shown to be inconsistent with the frequency distribution and wave vector orientations of the observed waves. A new theory involving Doppler-shifted lower hybrid waves driven by beamlike distributions of water ions near the space shuttle is developed using linear theory. This linear theory can explain generation of waves with (1) frequencies ranging from near zero frequency to the lower hybrid frequency, (2) wave vectors essentially perpendicular to the magnetic field, (3) wavenumbers increasing with wave frequency, and (4) wavelengths observable by the PDP antenna. These characteristics are all consistent with the observed properties of the waves, thereby providing strong support for the theory. In addition, the theory permits two qualitative explanations for the $V_\parallel/V_T$ effect. However, the linear theory cannot explain the details of the observed frequency spectrum of the waves. Strong, qualitative arguments that the effects of spatial inhomogeneity and nonlinear effects should modify the predicted linear spectrum are presented. In particular, the observed ratio of wave energy to thermal plasma energy is of order 10^{-5}, sufficient for nonlinear and strong turbulence effects to be potentially important. Lastly, the observed $V_\parallel/V_T$ effect implies optimum conditions for use of the space shuttle as a base for observing plasma waves generated by active experiments or natural ionospheric waves. Ideally, the shuttle's orbit should be designed so that $V_\parallel/V_T$ exceeds about 0.7, thereby favoring polar orbits and arguing against equatorial orbits. Alternatively, free-flying experiments should be used.

1. INTRODUCTION

One of the unexpected results from the OSS 1 mission was the observation of high levels of broadband electrostatic waves in the very near vicinity of the space shuttle [*Murphy et al.*, 1983; *Shawhan et al.*, 1984]. These waves were observed using the plasma wave receiver on the Plasma Diagnostics Package (PDP) spacecraft. During this mission the PDP remained in the orbiter's payload bay or on the remote manipulator system (RMS) arm within about 10 m from the orbiter. The waves had their greatest spectral densities between 31 Hz (the lowest frequency measured) and about 31 kHz, with a peak between 100 Hz and 300 Hz, but extended in frequency above 100 kHz. In comparison, during this mission the ion gyrofrequency was of order 50 Hz, the lower hybrid frequency was of order 5 kHz, and the oxygen ion plasma frequency was of order 15–55 kHz. *Hwang et al.* [1987] suggested that these broadband electrostatic waves are driven by the secondary ion streams observed [*Stone et al.*, 1983, 1986] in the near vicinity of the orbiter. The relevant instabilities are the ion acoustic and ion-ion acoustic instabilities [e.g., *Gary and Omidi*, 1987]. Hwang et al. claimed that these theoretical ideas predicted waves with frequencies in good agreement with the observational data of *Murphy et al.* [1983] and *Shawhan et al.* [1984].

The PDP spacecraft performed further investigations into the shuttle's interaction with the ionosphere during the Spacelab 2 mission. This mission, launched on July 29, 1985, had a nearly circular, low-inclination orbit with a typical altitude of 320 km and an inclination of 49.5°. In preparation for the Spacelab 2 mission, steps were taken to reduce the noise level of the plasma wave receivers on the PDP. The PDP probed the shuttle's environment both while attached to the spacecraft on the RMS arm (distances less than about 10 m) and while flying free of the shuttle (the so-called "free-flight" mission) out to distances of order 400 m. While the PDP was on the RMS arm, the shuttle performed a roll maneuver (the XPOP (X perpendicular to the orbital plane) roll) designed to allow investigation of the broadband near-zone waves as a function of phase relative to the orbiter's velocity vector. The free-flight mission included two complete fly-arounds of the shuttle orbiter, including two pairs of

Paper number 91JA00982.
0148-0227/91/91JA-00982$05.00

transitions from the region downstream of the shuttle (defined by the orbiter's velocity relative to the ionospheric plasma) to the upstream region. Previous papers discussing plasma wave data from the Spacelab 2 mission include those of *Gurnett et al.* [1988], *Tribble et al.* [1989], and *Cairns and Gurnett* [1991].

This paper focuses on the observation and theory of plasma waves in the very near vicinity (within 10 m) of the space shuttle during the Spacelab 2 mission. The observational data presented are from the XPOP roll period and from one upstream-downstream transition during the free-flight period. These data allow demonstration of the control of the amplitude and spectral characteristics of the near-zone waves by the angle between the orbiter's velocity vector and the magnetic field direction (section 2), the so-called $V_\parallel/V_T$ effect, analogous to the results of *Cairns and Gurnett* [1991] for some waves during the free-flight mission. Detailed investigations into the spectral characteristics of the near-zone waves are undertaken. These investigations reveal that the wave spectrum is most plausibly composed of three components: a uniform component covering the frequency range from 30 Hz to about 10 kHz, together with superposed components near about 100 Hz and near the lower hybrid frequency (~5–10 kHz). Comparisons are made with the results of *Murphy et al.* [1983] and *Shawhan et al.* [1984]. Variations in the wave characteristics with roll phase are briefly discussed in section 3. Section 4 contains data from a period in which the PDP moves from upstream to downstream of the shuttle while magnetically connected. These data suggest that the near-zone waves have wave vectors approximately perpendicular to the magnetic field. Theoretical discussions of the near-zone waves are presented in sections 5 and 6. The theories of *Hwang et al.* [1987] and *Papadopoulos* [1984] are discussed in section 5. Arguments are presented that neither theory can explain the observed waves. A new theory involving Doppler-shifted lower hybrid waves driven by pickup water ions via the modified-two-stream instability [*Krall and Liewer*, 1971; *Papadopoulos*, 1984] is suggested for the general characteristics of the broadband near-zone waves. These pickup water ions are produced by charge exchange interactions between ionospheric oxygen ions and water molecules outgassed from the space shuttle [*Paterson and Frank*, 1989; *Cairns* 1990]. This theory differs from Papadopoulos' theory principally in the source of the ion beam driving the waves. A linear theory is developed that is capable of explaining growth of waves with many of the observed characteristics, in particular the "uniform" broadband component of the waves. The theory is consistent with the inferred wave vector directions and two natural interpretations for the $V_\parallel/V_T$ effect. However, the theory cannot presently explain the low-frequency and lower hybrid frequency components of the wave spectrum. Suggestions are made and discussed that nonlinear effects and the effects of spatial inhomogeneity produce the detailed frequency structure of the observed waves. Further discussion, in particular the implications of the $V_\parallel/V_T$ effect described in section 2 for design of future shuttle missions, is given in section 6, followed by the conclusions of the paper in section 7.

2. Observations of the Near-Zone Waves During the XPOP Roll

The results presented in this paper are from the Helios and MFR (medium-frequency receiver) subsystems of the plasma wave receiver on the PDP spacecraft [*Shawhan*, 1982; *Gurnett et al.*, 1988]. The Helios instrument measures narrowband electric field signals from 31.1 Hz to 178 kHz using 16 logarithmically spaced channels, four per frequency decade. The frequency bandwidths are nominally ±15% below 1 kHz and ±7.5% above 1 kHz. Eight additional higher-frequency channels from 311 kHz to 17.8 MHz constitute the MFR subsystem. A double-sphere antenna is used with these instruments. The sphere separation (and effective antenna length) is 1.15 m while on the RMS arm (e.g., during the XPOP roll) and 3.89 m during the free-flight mission. The diameter of each sphere is 10 cm. Each channel provides a data point each 1.6 s; both peak and average signals during each measurement interval are recorded. Only the average values are presented here.

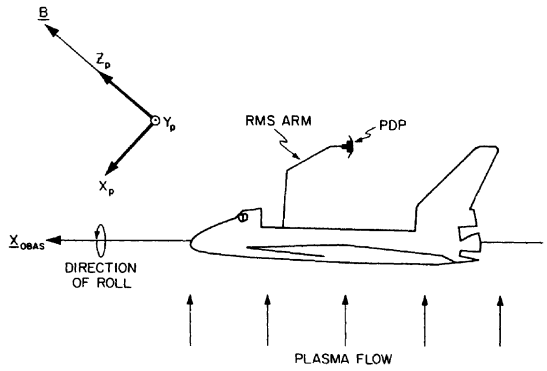

Fig. 1. The geometry of the XPOP roll during the Spacelab 2 mission. The shuttle rolls about the nose-tail or X_{OBAS} axis while its orbital velocity is perpendicular to the X_{OBAS} axis. The "pickup" coordinate system X_P-Y_P-Z_P is also defined.

The geometry of the XPOP roll is described in Figure 1. The PDP is attached to the RMS arm and remains in the same position (but in various orientations) relative to the orbiter during the XPOP roll. At about 0134 UT, thruster firings induce the orbiter to roll around the X_{OBAS} axis, corresponding to the nose-tail axis of the orbiter, with the orbiter oriented so that the X_{OBAS} axis is essentially perpendicular to the shuttle's orbital motion around the Earth. Accordingly, the orbiter rotates about an axis perpendicular to the ram velocity direction. This rotation is designed to move the PDP into the orbiter's wake region and upstream region at a constant distance and position relative to the orbiter. The rotation rate is 0.933° s^{-1}, corresponding to one wake transit about every 6 min.

Plate 1*a* shows a spectrogram formed from Helios and MFR data with spectral density (in V^2 m^{-2} Hz^{-1}) color-coded for the time period of the XPOP roll during the Spacelab 2 mission: 0134–0240, day 212, 1985. The lower black curve is the lower hybrid frequency computed as the product of the square root of the electron to (oxygen) ion mass ratio times the electron gyrofrequency (upper black curve). For comparison, nominal plasma parameters for the XPOP roll period, including the oxygen ion plasma frequency and gyrofrequency, are given in Table 1. The data invariably show the highest spectral densities at low frequencies below 1 kHz and the lowest spectral densities at high frequencies of order 100 kHz and above. Many depletion

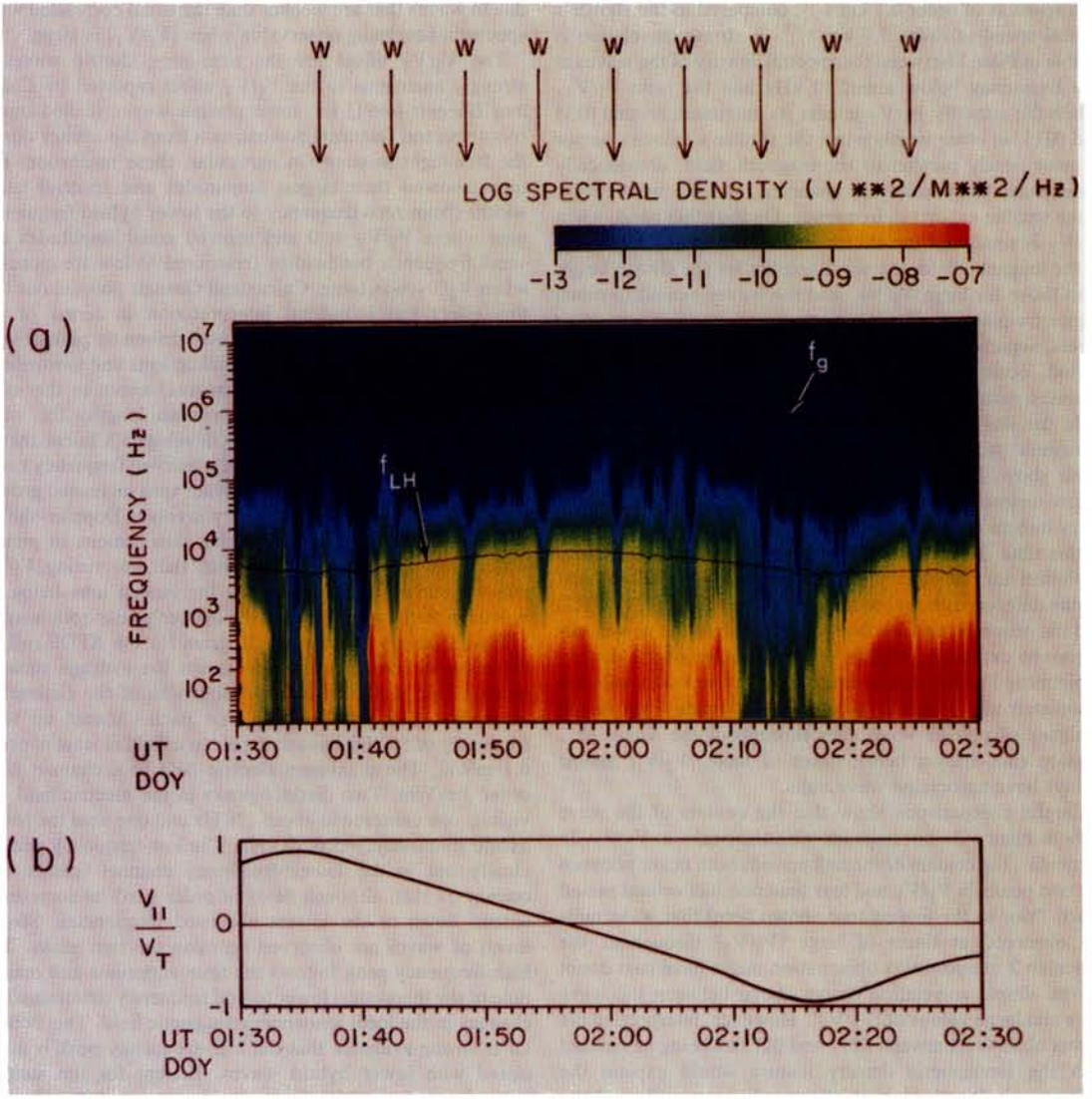

Plate 1. (*a*) A Helios-MFR color spectrogram for the period of the XPOP roll. Spectral density is color-coded. Black lines show the variation in the electron gyrofrequency f_g and the lower hybrid frequency f_{LH}. (*b*) The variation in the quantity $V_\parallel/V_T$, measuring the ratio of the shuttle's orbital velocity parallel to the magnetic field and the orbital speed, during the XPOP roll. The nulls in the wave data are correlated with large values of $V_\parallel/V_T$.

features are visible in the data, including the event near 0140:00 (hour-minute:second of universal time) and the periodic events marked with arrows at 0148:40, 0154:40, etc. These 6-min period events are associated with the PDP's motion through the orbiter's plasma wake, and the arrows mark the times when the PDP is in the center of the orbiter's wake. The features at 0134 and 0140 occur while the PDP is directly upstream (in the ram direction) from the orbiter. Correlations between the wave characteristics and the PDP's phase (or position) relative to the velocity vector are discussed briefly in the next section. The present section is devoted to discussion of more general characteristics of the waves.

Plate 1*b* shows the variation in the quantity $V_\parallel/V_T$ for this time period. We define the quantities $V_\parallel$, $V_\perp$, and V_T as the components of the orbiter's velocity vector (relative to the ionospheric plasma) parallel and perpendicular to the magnetic field and the orbiter's speed, respectively. Corotation of the ionospheric plasma is assumed: the plasma's corota-

TABLE 1. Nominal XPOP Roll Parameters

Parameter	Value
n_e	10^4–6×10^5 cm^{-3}
T_e	2000 K
T_O	1000 K
f_{gO}	20–45 Hz
f_{LH}	4–8 kHz
f_{pO}/f_{gO}	100–2000

tion speed is of order 0.5 km s^{-1}, compared to the shuttle's orbital speed of order 7.8 km s^{-1}. A strong correlation is visible in Plate 1 between the spectral density of the waves at any frequency below about 10 kHz and the ratio $V_\parallel/V_T$. When the quantity $V_\parallel/V_T$ is near its maximum around 0135 and 0215, in other words when the shuttle's velocity vector is most nearly parallel to the magnetic field, dramatically lower wave amplitudes are observed, and the waves have much smaller extents in frequency. On the other hand, when $V_\parallel/V_T$ is small and the shuttle moves almost perpendicular to the magnetic field, the wave amplitudes are always larger than those for large $V_\parallel/V_T$, and the waves extend to much higher frequencies. Two distinct periods of very low wave levels, separated by less than one-half the shuttle's orbital period, occur near the peaks in $V_\parallel/V_T$. This fact argues against a peculiar region of ionospheric plasma being responsible for this phenomenon. Density data from the PDP's Langmuir probe (J. S. Pickett, personal communications, 1990) show, however, that the electron density decreases below measurable levels between 0214 and 0221, indicating entry into an unusually low density region of the ionosphere at this time. Nevertheless, the absence of a similar density depletion for the first plasma wave null (0132–0141) and timing differences between the second wave null (0211–0217) and the observed density depletion show that the wave nulls cannot be explained in terms of unusual ionospheric density depletions. Further strong evidence that the wave nulls are associated with times of large $|V_\parallel/V_T|$ comes from recent analyses of plasma wave data throughout the Spacelab 2 mission (not shown here): times of large $|V_\parallel/V_t|$ almost always have associated wave nulls.

Careful comparisons show that the centers of the wave nulls in Plate 1 do not coincide with the peaks in $V_\parallel/V_T$. In particular, the centers of the null periods both occur between the two peaks in $V_\parallel/V_T$ and less than one-half orbital period apart. Prior to the finding (not shown here) that wave nulls are observed at times of large $|V_\parallel/V_T|$ throughout the Spacelab 2 mission, this observation might have cast doubt on the simple correlation drawn above between the wave nulls and large values of $|V_\parallel/V_T|$. However, interpreting the waves observed between 0217 and 0219 as being associated with the ionospheric density feature would explain the difference in length (2 min) of the two wave nulls and the failure of the second wave null to include the peak in $V_\parallel/V_T$ (in contrast to the first null period). Some support for this interpretation comes from observations of plasma waves associated with a similar ionospheric density depletion during the free-flight mission (not shown here). This interpretation therefore significantly strengthens the correlation drawn above between wave nulls and large values of $|V_\parallel/V_T|$ in Plate 1. Furthermore, we note that some relatively strong, transient wave features occur during the first wave null which are not directly associated with thruster firings. Thruster firings occur at 0134:1,2,3,44,45, 0136:7,15,16,59, 0137:0–4,48–50, 0138:17–18, 0140:42–45, and 0144:34. Accordingly, the waves preceding the firings at 0136 and the waves during minute 0139 are not directly thruster-associated. These waves do not appear to be part of the usual orbiter-associated spectrum and may be associated with particular roll phases of the orbiter and the attitude of the PDP spacecraft itself. Thus these phase complications between the wave nulls and the peaks in $/V_\parallel/V_T$ may also be due to waves that are weaker than the usual correlated wave spectrum becoming observable when $|V_\parallel/V_T|$ is large.

The $V_\parallel/V_T$ effect for the near-zone shuttle waves is strongly analogous to the $V_\parallel/V_T$ effect reported by *Cairns and Gurnett* [1991] for some plasma waves (called mushroom spectral features) downstream from the orbiter during the free-flight mission. In particular, these mushroom features showed their largest amplitudes and spectral bandwidths (from zero frequency to the lower hybrid frequency) near where $V_\parallel/V_T = 0$ and showed small amplitudes and small frequency bandwidths (restricted to low frequencies) when $V_\parallel/V_T$ was large. Cairns and Gurnett pointed out that this effect has a natural interpretation in terms of the optimum conditions for wave growth driven by pickup ions. In particular, when $V_\parallel = 0$ the pickup ions and ionospheric plasma (convecting the plasma waves) move in the same plane, thereby permitting longer path lengths for wave growth. Cairns and Gurnett also developed a linear theory capable of explaining waves in the observed frequency range and broadening of the wave spectrum with increased growth lengths for the waves. This theory involves Doppler-shifted lower hybrid waves driven by ring distributions of pickup water ions. One might infer, then, that the strong $V_\parallel/V_T$ effect reported here is evidence for pickup ions being involved with the generation of the orbiter's near-zone waves.

Plate 2 shows another spectrogram for the XPOP roll; in this case the color coding represents the average squared electric field in the frequency bandwidth of the channel at frequency f. It can be seen that each channel up to a frequency of 56 kHz has an rms electric field at least of order 0.1 mV/m. The maximum electric field in a channel is of order 3 mV/m. Two distinct peaks in the electric field are visible: one centered at about 178 Hz and one near the lower hybrid frequency, ~5.6–10 kHz. The low-frequency peak is clearly not in the lowest-frequency channel (center frequency 31 Hz), although fields of order 1 mV/m sometimes extend down to the lowest observed frequencies. Strong levels of waves are observed between the two peaks. The high-frequency peak follows the time variations and magnitude of the theoretical lower hybrid frequency determined by changes in the local ionospheric magnetic field. This behavior is strong evidence that the high-frequency peak is associated with lower hybrid waves. Except for the sudden extensions of the high-frequency waves to 178 kHz discussed briefly in the next section, e.g., at 0141:40, 0147:00, and 0158:30, the high-frequency waves only have significant spectral densities up to about 56 kHz.

Murphy et al. [1983] and *Shawhan et al.* [1984] have previously recognized the existence of the low-frequency peak. However, the peak near the lower hybrid frequency has not been identified before in the near-zone data. The presence of strong low-frequency waves and a high-frequency peak near the lower hybrid frequency is strongly reminiscent of the plasma waves observed during the free-flight mission [*Gurnett et al.*, 1988; *Cairns and Gurnett*, 1991]. In particular, Plate 1 of Cairns and Gurnett's paper shows the presence of strong waves at low frequencies together with a high-frequency band near the lower hybrid frequency. This strong similarity provides a further hint that these near-zone waves are driven by pickup ion instabilities, as is presently believed for the aforementioned waves observed during the free-flight mission.

The presence of two peaks in the wave spectrum is also

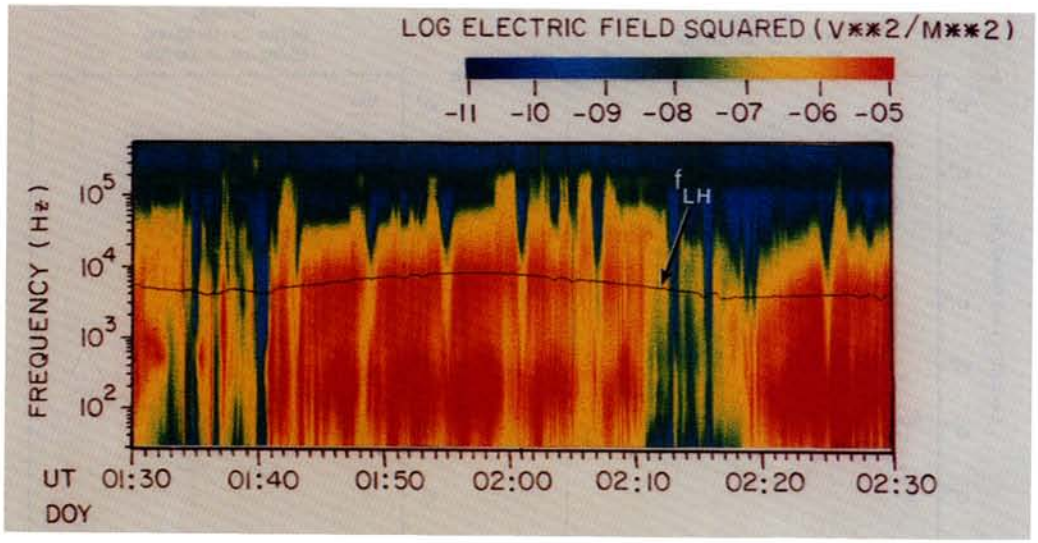

Plate 2. Spectrogram of Helios-MFR data showing the color-coded squared electric field measured in each channel bandwidth. Two peaks are evident, one near 100 Hz and one at the lower hybrid frequency.

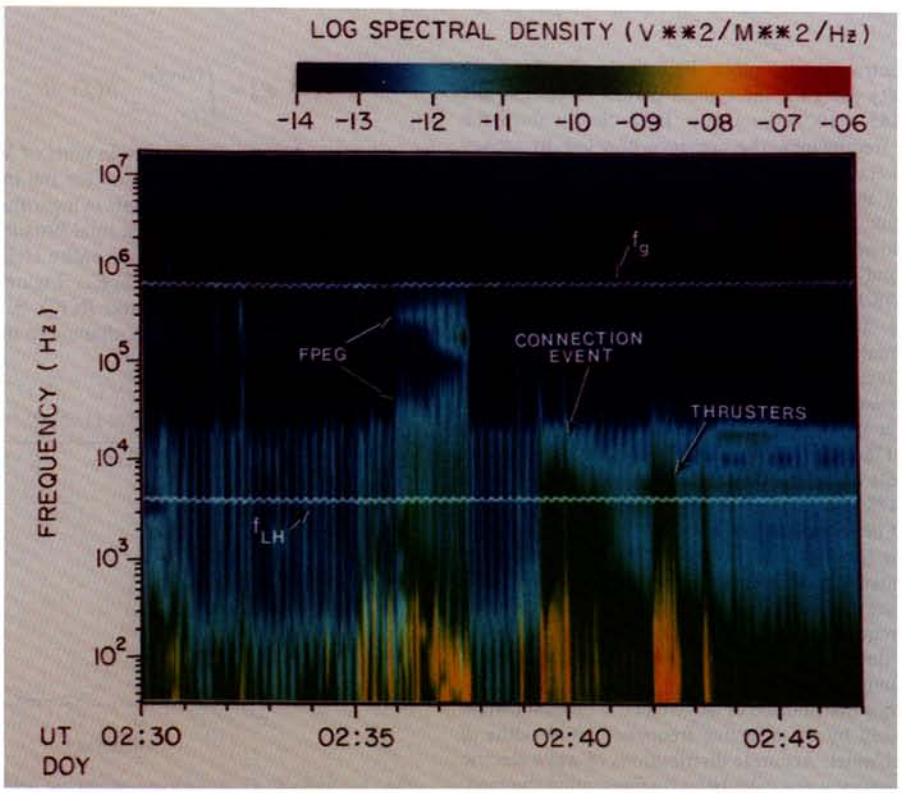

Plate 3. A Helios-MFR spectrogram for the period 0230–2407, day 213, during the free-flight mission. Spectral density is color-coded. White lines show the electron gyrofrequency and lower hybrid frequency. Signals associated with spacecraft interference, the FPEG experiment, and thruster firings are indicated in the figure and text. The signals marked "connection event" occur while the PDP is magnetically connected to the space shuttle. These data are interpreted in terms of observations of the shuttle's near-zone waves, implying that these waves are flutelike modes with wave vectors approximately perpendicular to the magnetic field.

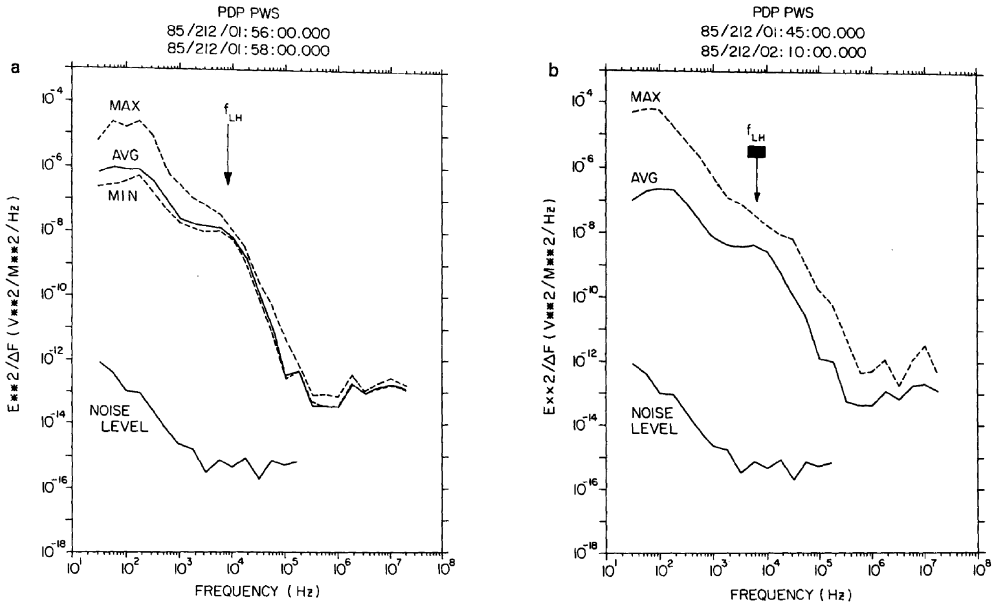

Fig. 2. (*a*) Spectral density as a function of channel frequency for the period 0156–0158 UT during the XPOP roll. The solid curve shows the average spectral density, while the long- and short-dashed curves show the maximum and minimum observed spectral densities, respectively, during this period. The lowest line shows the calibrated receiver noise level (before launch). (*b*) Similar to Figure 2*a*, but for the period 0145–0210.

visible in spectral density plots. Figures 2*a* and 2*b* show spectral density plots for the typical period 0156–0158 and the period 0145–0210, respectively. Both clearly show the falloff at low frequencies, the presence of a low-frequency peak near 178 Hz, a region with spectral densities decreasing approximately inversely with frequency between the low-frequency peak and the lower hybrid frequency, a bulge around the lower hybrid frequency marking the second component, and a rapid falloff at higher frequencies. Channels above 178 kHz (in the MFR) show essentially background levels. The rapid falloff at high frequencies is believed to be real: the whistler mode emissions seen during some FPEG (fast pulse electron gun) events on the free-flight missions [*Gurnett et al.*, 1988; *Farrell et al.*, 1989] show no evidence for a significant difference in sensitivity between the 100- and 178-kHz Helios channels and the 311-kHz and higher channels of the MFR. In addition, ignoring the usual spike in the 178-kHz channel at low signal levels (e.g., the constant light blue band at 178 kHz in Plate 1), we see that the decreasing trend in the 10- to 100-kHz Helios channels plausibly connects to the very low levels seen in the MFR channels. However, we note that this falloff may also be due to the high-frequency portion of the wave spectrum being undetectable due to the wavelengths being very short relative to the antenna length.

The frequency distribution of wave electric fields shown in Plate 2 is biased by the effective frequency bandwidths of each Helios channel. Accurate distributions of wave electric fields with frequency are calculated by integrating the measured spectral densities over frequency intervals centered on, but spanning the entire frequency ranges between, Helios channels. We define the broadband electric field for the waves in the frequency range centered on the nth channel, E_n, by

$$E_n^2 = \int_{(f_n f_{n-1})^{1/2}}^{(f_n + 1 f_n)^{1/2}} S(f)\, df. \qquad (1)$$

Here $S(f)$ is the spectral density in units of $V^2\ m^{-2}\ Hz^{-1}$, and the frequency intervals chosen for the integration correspond to equally spaced intervals in logarithmic frequency centered on the nth channel. The total broadband, frequency-integrated electric field over the entire Helios frequency, E_T, is then defined by $E_T = \Sigma_n E_n$. Figure 3 shows the frequency distribution of the ratio $R(f_n) = E_n/E_T$ of the electric field centered on the nth channel to the total broad-

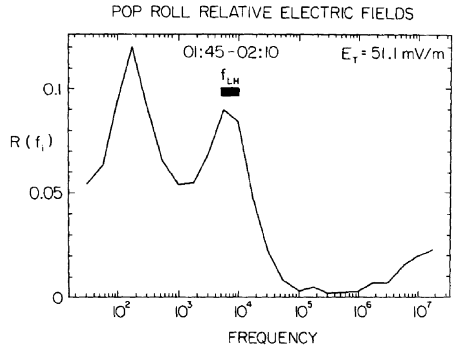

Fig. 3. Ratio $R(f)$ of the average electric field in a frequency bandwidth divided by the total average broadband field as a function of frequency (see text for a detailed definition). The wave fields are essentially constant from 30 Hz to 10 kHz and sharply lower at higher frequencies, reaching the background level by 100 kHz. Two peaks, by a factor of 2, are seen in the average wave fields: one at low frequencies near 178 Hz, and one at the lower hybrid frequency.

band electric field. The data plotted are for the period 0145–0210 shown also in Figure 2*b*. The total average broadband electric field E_T for this time period was 51.1 mV/m. Two peaks are visible, superposed on a uniform high level at frequencies below about 20 kHz. The first peak is centered at low frequencies near 178 Hz, with a broad shoulder at significant amplitudes to the second peak which is situated between 5.6 kHz and 10 kHz. As described above, the lower hybrid frequency varies between 5 and 10 kHz during this time period, providing an excellent identification for the higher-frequency peak. Above 56 kHz the measured electric fields are essentially negligible. We note now that the linear theory in section 6 predicts maximum wave growth at wavelengths of order 0.8 m, commensurable with the antenna length (1.15 m) for these observations. It is therefore likely that the broadband wave electric field estimated above (51 mV/m) is smaller than the actual field present in the plasma.

The interpretation of the data in Plates 1 and 2 and Figures 2 and 3 in terms of components in the wave spectrum is not unique. However, the peaks in Figure 3 are only a factor of 2 greater than the level between the peaks and at lower frequencies than the first peak. It therefore seems most appropriate to interpret the wave spectrum in terms of a fairly constant high level of waves (electric fields of order 2.5 mV/m per frequency interval) from 31 Hz to 10 kHz with two superposed peaks, one around 178 Hz and one near the lower hybrid frequency. These superposed peaks have electric fields a factor of 2 higher than the constant level of waves between 30 Hz and 10 kHz. These data require any high-frequency waves above about 20 kHz to smoothly merge with the lower hybrid frequency waves; no evidence is found for any sharply peaked wave components in the frequency range 10–40 kHz. These identifications are referred to below as the "uniform" component, the low-frequency component, and the lower hybrid component. We will show below (section 6) that a simple linear theory can explain growth of waves over a broad frequency bandwidth between zero frequency and the lower hybrid frequency, thereby providing an explanation for the uniform component. It is suggested below that the effects of nonlinearities and spatial inhomogeneities lead to the developments of the low-frequency and lower hybrid frequency enhancements. Despite the above interpretation adopted in this paper we recognize that an interpretation in terms of only two wave components with broad extents in frequency, one centered at 178 Hz and one at the lower hybrid frequency, is not precluded by the available observational data. No theoretical interpretation is presently available for this two-component interpretation.

3. Variations of the Near-Zone Waves With Roll Phase

The periodic patterns at the XPOP roll period in Plates 1 and 2 indicate that the plasma waves associated with the space shuttle show significant and often reproducible variations with position relative to the ram direction. Figure 4 shows the time variation of the phase angle ϕ between the ram direction and the PDP's position vector relative to the orbiter. Times when the PDP is directly in the orbiter's wake region ($\phi = 0°$) are denoted by white arrows in Plate 1. It is clear that the high-frequency null features occur when the

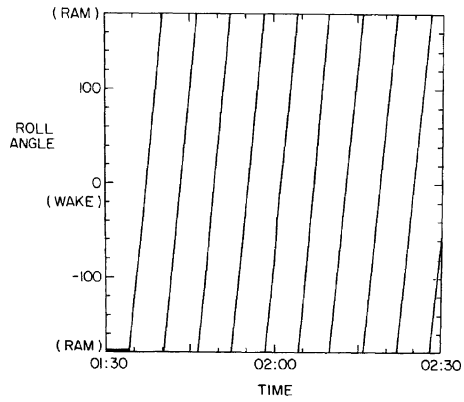

Fig. 4. Roll angle versus time for the period 0130–0230 during the XPOP roll. A phase angle of 0° corresponds to the PDP being in the center of the shuttle's wake.

PDP is in the orbiter's wake region [*Murphy et al.*, 1983]. *Tribble et al.* [1989] find that the low-frequency waves in the ranges 6–40 Hz also show a null region when the PDP is in the orbiter's wake. The characteristics of these null features have implications for the wavelengths of the waves, as we now argue. The important point to note is that the higher-frequency waves always decrease in amplitude before the lower-frequency waves when approaching the center of the shuttle's plasma wake, with increases in amplitude occurring in a symmetric fashion while leaving the wake center. This behavior is consistent with the higher-frequency waves having shorter wavelengths, thereby having greater difficulty propagating into the deep null observed in the plasma density [*Murphy et al.*, 1983; *Tribble et al.*, 1989] in the orbiter's wake. We will show that the theoretical model for the plasma waves developed in section 6 predicts this qualitative relationship between wave frequency and wavelength.

In distinction to the usual plasma wave null when the PDP is in the orbiter's plasma wake, it is usual for the wave intensities to be largest when the PDP is located directly upstream from the orbiter ($\phi = -180°$ or 180°). However, during the times of maximum $V_\parallel/V_T$, nulls in the plasma waves are seen when the PDP is in the ram direction (near 0134, 0140, and 0216) or in the wake. Low-level waves are observed at other roll angles during these periods.

Two further aspects of the near-zone plasma waves are deferred to future work. The first concerns the existence and characteristics of the low-frequency 6- to 40-Hz wave enhancements suggested by *Tribble et al.* [1989] to occur near where the PDP enters the shuttle's Mach cone. Consideration of Plates 1 and 2 provides little support for this suggestion; however, the survey slides for the PDP instruments clearly show Langmuir probe data supporting this notion for several wake transits. At present, no consistent trend in the data is apparent. Further work is warranted on this matter. The second topic deferred to the future involves the sudden extensions of the high-frequency waves to near 178 kHz visible, for example, near 0141:30 and 0158:30. At the present time we have no viable explanations for these events.

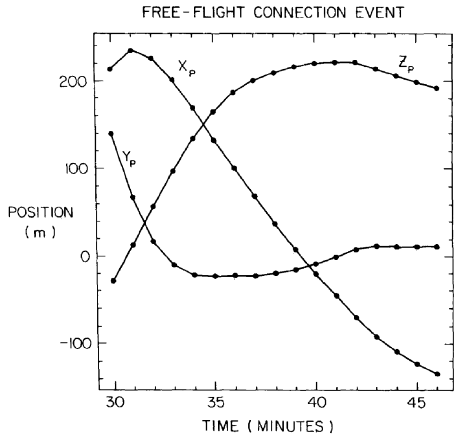

Fig. 5. Variations in the coordinates X_P, Y_P, and Z_P of the PDP relative to the space shuttle as a function of time for the data shown in Plate 3.

4. Observations of the Near-Zone Waves During the Free-Flight Mission

Plate 3 shows wave data from 0230 to 0247, day 213, 1985, during the PDP spacecraft's free-flight mission. The motion of the PDP in X_P-Y_P-Z_P coordinates is described in Figure 5. The "pickup" coordinate system X_P-Y_P-Z_P is defined by *Cairns* [1990]. The origin is situated at the orbiter's center of mass and moves with the space shuttle. The ionospheric magnetic field is directed along the Z_P axis, and the ionospheric plasma is constrained to move in the X_P-Z_P plane with velocity $(-V_\perp, 0, -V_\parallel)$. In contrast, the water pickup ions move in a cycloidal path in the X_P-Y_P plane with convection velocity $(-V_\perp, 0, 0)$ and gyrospeed of order $V_\perp$, together with thermal motions along the magnetic field. For future reference, at 0240, $V_\perp = -1.76V_\parallel$. A summary of the PDP's motion is as follows. The PDP is initially moving downstream from the upstream region with small Y_P at a large and approximately constant distance along the magnetic field (Z_P coordinate) of order 215 m. The PDP has position $X_P = 0$ near 0239:15 (i.e., the PDP is magnetically connected to the orbiter's center of mass) and $Y_P = 0$ near 0241:10 when downstream from the shuttle (i.e., probing the center of the wake).

FPEG interference is visible in Plate 3 as spikes extending from low frequencies to the electron gyrofrequency from about 0230 to 0238. Thruster firings occur frequently from 0225 to 0238, and thereafter at 0238:54, 0239:22,57, 0242:2–6,10,13,14,16,18,19,23,27,30–31, and 0243:12,16,57. However, plasma waves are observed in association with the upstream-downstream transition $X_P = 0$. A strong broadband burst of waves extending up to the lower hybrid frequency is observed as the PDP becomes magnetically connected to the space shuttle (i.e., $X_P = 0$). The maximum frequency of these broadband waves abruptly decreases from near the lower hybrid frequency to about 500 Hz at about 0241:00 and then tends to about 300 Hz with increasing distance downstream. At 0241:10 the PDP is magnetically connected to the center of the wake with $X_P \sim -50$ m, $Y_P \sim 0$, and $Z_P \sim 220$ m. Note the relative lack of waves between the lower hybrid frequency and 1 kHz from 0241:00 to 0241:30. Waves near the lower hybrid frequency start near 0241:30, leading into the mushroom spectral feature centered near 0302 discussed briefly by *Cairns and Gurnett* [1991]. Notice also the band of waves between 10 and 20 kHz from about 0243 to 0247. This band is not discussed further in this paper; we note that these waves have frequencies near the oxygen plasma frequency implied by the Langmuir probe data (of order 14–9 kHz at the above times) and frequencies of order 3 times the lower hybrid frequency.

The important observation here is the onset of strong waves at frequencies up to and above the lower hybrid frequency when the PDP becomes magnetically connected to the space shuttle. Inspection of the PDP survey slides indicates no obvious increases in electron or ion fluxes measured by the LEPEDEA, retarding potential analyzer (RPA), ion mass spectrometer (IMS), or other particle instruments or changes in the dc electric field. It does not appear correct, therefore, to interpret the observed plasma wave event in terms of waves generated in the vicinity of the PDP due to particles originating at the space shuttle. Electrostatic waves with wave vectors perpendicular to the magnetic field have wave fronts aligned along the magnetic field. That is, the electric field of such a wave does not vary along the magnetic field in an infinite homogeneous plasma. We therefore interpret the burst of waves observed between 0239:30 and 0241:00 in terms of the intense waves generated in the near vicinity of the space shuttle being observed along the magnetic field from the shuttle. This implies that the near-zone waves, at least at frequencies below a few times the lower hybrid frequency, have wave vectors oriented perpendicular to the magnetic field. This interpretation places significant restrictions on theories attempting to explain the near-zone waves. The evident decrease in amplitude for the free-flight waves compared with the near-zone waves, and the restriction in the frequency spectrum of the waves, may be qualitatively explained in terms of the inhomogeneous plasma environment of the shuttle and the smaller wavelengths for the higher-frequency waves inferred from the high-frequency nulls in the orbiter's wake (see last section). We now proceed to gather additional supporting evidence for our interpretation of the wave vectors of the near-zone waves.

Figure 6 compares the spectral density of the burst of waves for the time period 0239:40–0239:50, day 213, with the average spectral density of the near-zone waves shown in Figure 2*b* (time period 0145–0210, day 212). These spectral density profiles are surprisingly similar. The free-flight data show two low-frequency peaks, one near 178 Hz and one near the lower hybrid frequency of about 3 kHz, which compare well with the XPOP roll observations. Note that the lower hybrid frequency during this period of near-zone data was above about 5 kHz, consistent with the frequency of the second peak. The high-frequency falloff above the lower hybrid frequency shows similar forms in both the free-flight and near-zone data. These spectral density profiles coincide well if one multiplies the free-flight curve by a factor of 50, corresponding to electric fields a factor of 7 stronger. These spectral density profiles are therefore consistent with the interpretation that the observed free-flight signals are plasma waves generated in the near-zone region with wave vectors perpendicular to the magnetic field (i.e., flutelike modes). In addition, in section 6 we show that the linear theory predicts maximum growth at wavelengths of order 1 m: the longer

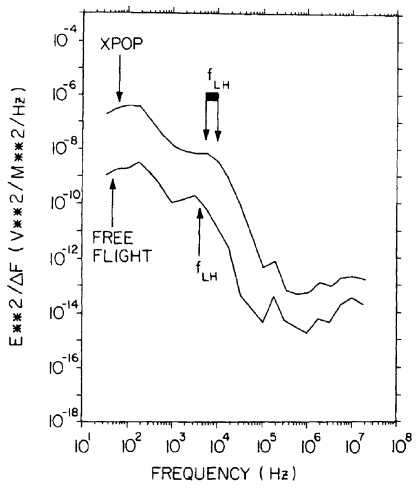

Fig. 6. Comparisons of the spectral density profiles of the waves observed during the free-flight connection event (0239:40–0239:50, day 213) and during the XPOP roll (0145–0210, day 212). These curves are qualitatively similar with magnitudes differing by a factor of order 50 (the antenna lengths differ by a factor of order 3). These data support the interpretation that the connection event corresponds to observation of the near-zone waves at a 200-m distance along the magnetic field, implying that the near-zone waves are flutelike modes.

antenna length during free flight (3.89 m) compared with the XPOP roll (1.15 m) then implies less efficient measurement of the wave electric fields. An additional point of interest involves the extension of the wave spectrum to 20 kHz in the free-flight data when the lower hybrid frequency is of order 3 kHz. During the free-flight mission it is unusual to observe waves above about 2 times the lower hybrid frequency (except for thruster- and FPEG-associated waves and the interference spikes) except perhaps well downstream in the wake region. Thus the observation of waves above about 10 kHz during this connection event provides some weak additional support for the interpretation in terms of the broadband near-zone waves advanced above. Evidence for spin modulation of the waves was sought to provide further support for the wave vector directions inferred above. However, except for a spacecraft-associated signal with one maximum-null pair per spacecraft rotation, the data showed no evidence of consistent spin modulation.

Another event similar to the 0239 upstream-downstream transition occurred near 0203. This time the transition is from downstream to upstream. For this event, $V_\perp = 3.3V_\parallel$, and the lower hybrid frequency is of order 8 kHz. The wave spectrum is observed to continue up to about 56 kHz, well above the lower hybrid frequency and the interference spikes at this time. This spectrum provides further support that the PDP is observing the broadband near-zone waves during this event, and thereby that the near-zone waves have wave vectors oriented essentially perpendicular to the magnetic field up to frequencies at least 4 times the lower hybrid frequency.

5. Previous Theories for Near-Zone Waves

5.1. *Discussion of Hwang et al.'s Theory*

Hwang et al. [1987] suggest a linear theory for these electrostatic, broadband near-zone waves on the basis of the observations of *Murphy et al.* [1983] and *Shawhan et al.* [1984]. This theory involves (electron-ion) ion acoustic and ion-ion acoustic instabilities [e.g., *Omidi*, 1985; *Gary and Omidi*, 1987] driven by the secondary ion streams observed [*Stone et al.*, 1983, 1986] in the near vicinity of the space shuttle. Hwang et al. solve the electrostatic dispersion equation with Maxwellian distributions of magnetized ionospheric electrons, unmagnetized ionospheric oxygen ions, and an unmagnetized species of ions which drift relative to the ionospheric plasma particles and to the space shuttle. This last species represents the secondary ion stream. At the present time the origin and detailed characteristics of these secondary ion streams are not known (see, however, *Stone et al.* [1983, 1986]). Published plasma characteristics for the ion streams are few. Hwang et al. state that these streams have temperatures of a few hundred degrees Kelvin (similar to the expected temperature, ~300 K, of water molecules outgassed from the shuttle) and have current densities of order 30–70% of the ionospheric ram current. These current densities imply that the ion streams have number densities of order 30–70% of the observed ionospheric plasma flow's number density. Hereafter, the secondary ion stream is referred to as the ion beam.

Hwang et al. [1987] claim that their linear theory gives results which are consistent with the wave observations of *Murphy et al.* [1983] and *Shawhan et al.* [1984]. In this section we show that Hwang et al.'s theory is not consistent with the detailed properties of the broadband waves identified in this paper. In brief, Hwang et al.'s paper implies the following characteristics for the unstable waves and their corresponding instabilities: (1) The instabilities are the (electron-ion) ion acoustic and ion-ion acoustic instabilities [e.g., *Omidi*, 1985; *Gary and Omidi*, 1987]. (2) The instabilities are essentially unmagnetized (no mention is made of the angle between the magnetic field and the wave vector being important). (3) The important variable determining the angular characteristics of the unstable waves is $\theta = \cos^{-1}(\mathbf{k} \cdot \mathbf{v}_b)$, where $\mathbf{v}_b$ is the drift velocity of the secondary ion stream relative to the ionospheric plasma. (4) The unstable waves have wave vectors concentrated near $\theta = 0°$ or 77° depending on the ion stream density, temperature, and instability considered. (5) The maximum growth rate for the ion-ion acoustic instability dominates that for the electron-ion acoustic instability by a factor of at least 2 for relative beam densities less than 95%. (6) The growth rate of the waves as a function of wave frequency shows a single well-defined maximum at frequencies of order 10–50 kHz and essentially negligible wave growth below 1 kHz. (7) Decreasing the relative ion stream number density from its maximum value (100%) moves the peak in the growth rate from a wave frequency of 10 kHz to higher wave frequencies of order 50 kHz (50%) and above. (8) Ion streams with relative number density less than about 10% do not show effective growth. We note that Hwang et al.'s Figures 2 and 3 actually show plots of the growth rate versus the observable (PDP frame) wave frequency $f = \omega/2\pi$ and not the angular wave frequency ω (K. S. Hwang, personal communication, 1990).

We have reproduced Hwang et al.'s linear instability analysis and have verified points 1–6 above for Hwang et al.'s parameters. Disagreements between these first six theoretical results and the characteristics of the observed waves (see previous three sections) are now described. Elsewhere we present a detailed parameter analysis of Hwang et al.'s linear theory, considering in detail the unstable wavelengths and frequencies of the waves and the effects of different beam temperatures and plasma densities (I. H. Cairns, manuscript in preparation, 1991, hereafter referred to as C91). First, and most importantly, Figure 3 shows strong wave levels below 1 kHz, whereas Hwang et al.'s theory predicts essentially negligible growth rates below 1 kHz ($\gamma \leq \Omega_O$ where Ω_O is the angular oxygen ion gyrofrequency). Thus Hwang et al.'s theory cannot explain the portion of the observed uniform component below 1 kHz or the low-frequency component near 178 Hz. Second, Hwang et al.'s theory involves waves with no preferred orientation relative to the magnetic field, thereby being inconsistent with the observed waves having wave vectors essentially perpendicular to the magnetic field: (1) The ion-ion acoustic instability should produce waves with wave vectors lying on cones at large angles of order 75° relative to the beam velocity, and so in general at no common angle relative to the magnetic field direction. The ion-ion acoustic instability dominates the electron-ion acoustic instability except under relatively extreme conditions. (2) The electron-ion acoustic instability should produce wave vectors aligned approximately with the beam velocity, which itself is not expected, a priori, to be oriented perpendicular to the magnetic field. Third, Hwang et al.'s theory cannot explain the observed wave component localized near the lower hybrid frequency since the theory predicts essentially unmagnetized waves with no dependence on or importance for the lower hybrid frequency and the magnetic field strength. Fourth, Hwang et al.'s theory predicts a localized peak in the wave energy at frequencies of order 10–50 kHz that has no dependence on the magnetic field strength. The wave data show no evidence for such waves. However, in the C91 paper we show that Hwang et al.'s parameters imply that the peak growth rates actually occur at wavelengths too small to be observable by the PDP's double-sphere antenna (wavelengths smaller than or comparable to the sphere diameter). In fact, the dominant ion-ion instability has major difficulties in producing waves with significant growth rates at observable wavelengths.

A further major problem for Hwang et al.'s theory involves the temperature ratios chosen for the instability analysis. Ion acoustic and ion-ion acoustic instabilities are strongly dependent on the electron-to-ion and ion-beam temperature ratios T_e/T_i and T_i/T_b being sufficiently large [e.g., *Gary and Omidi*, 1987] for growth to overcome damping. Hwang et al.'s stated beam temperature of a few hundred degrees may be a lower limit due to instrumental limitations (N. H. Stone, personal communication, 1990). We note that there are theoretical difficulties in extracting such cold beams from the ionospheric oxygen plasma ($T_O \geq$ 1000 K), while pickup water ions are expected to have thermal temperatures of approximately 300 K. Hwang et al.'s temperature ratios imply ion and electron temperatures significantly out of the usual ranges for beam temperatures greater than about 150 K: a beam temperature of 200–300 K with $T_O/T_b = 7.5$ and $T_e/T_i = 2$ leads to oxygen ion temperatures $T_O \sim$ 1500–2250 K and electron temperatures

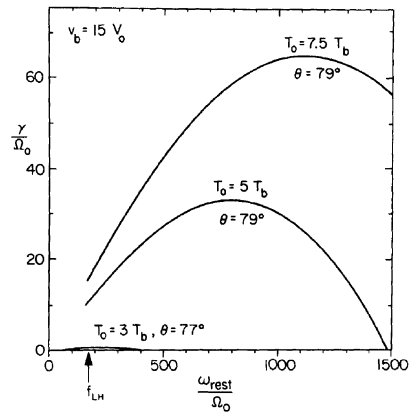

Fig. 7. Suppression of *Hwang et al.*'s [1987] ion-ion acoustic instability on varying the temperature ratio T_O/T_b from 7.5 to the more nominal value of 3. The other plasma parameters are appropriate to Hwang et al.'s Figure 2; v_b and V_O are the ion beam speed and the oxygen ion thermal speed, respectively. The plotted curves compare the growth rate and frequency (in the background plasma frame) of the waves for the value of θ with the maximum growth rate. Additional definitions of the plasma parameters are given in section 6.

$T_e \sim$ 3000–4500 K. In contrast, nominal ionospheric temperatures are $T_O \sim$ 1000 *K* and $T_e \sim$ 2000 K. During the PDP free-flight mission the oxygen ion temperature inferred from the RPA instrument's data [*Reasoner et al.*, 1986] is of order 1100 K whenever confidence may be attached to the fitting routine (D. L. Reasoner, personal communication, 1989). Use of nominal ion and electron temperatures in the linear theory is important since the near-zone waves are observed continuously (except when $V_\parallel/V_T \sim 1$). Taking T_b = 300 K, the nominal values for the ratio T_O/T_b lie in the range 3–4 with $T_e/T_O = 2$. In Figure 7 (and the C91 paper) we show that reducing the oxygen ion-beam temperature ratio from Hwang et al.'s value of 7.5 to the more conservative value of 3 leads to suppression of the (dominant) ion-ion acoustic instability. Thus, unless the beam temperatures are indeed significantly less than 300 K, we expect suppression (or at best slow growth) of Hwang et al.'s instabilities in the shuttle environment. Similarly, in the C91 paper we show that Hwang et al.'s instabilities are strongly dependent on the ratio of the electron plasma frequency to the electron gyrofrequency: the maximum growth rate for the ion-ion instability scales with the plasma frequency. A smaller, more typical plasma density than that quoted by Hwang et al. leads to significantly smaller growth rates for Hwang et al.'s instabilities. Finally, the absence of a direct interpretation for the $V_\parallel/V_T$ effect described in section 2 constitutes a further problem for Hwang et al.'s theory.

In summary, Hwang et al.'s theory is unable to account for the intense, broadband near-zone waves at frequencies below several times the lower hybrid frequency. It is possible that Hwang et al.'s theory may apply to the low-level broadband waves above about 20 kHz or to the high-frequency extension events near 0141:30 and 0158:30 for example. Detailed discussions of these possibilities and the above results are provided in the C91 paper. We note that in contrast to the Hwang et al. theory the lower hybrid wave

theory introduced in section 6 naturally predicts the generation of waves with strong growth rates in the observed frequency range, observable wavelengths, wave vectors essentially perpendicular to the magnetic field, and characteristics that are relatively independent of the assumed beam temperature and plasma density.

5.2. *Discussion of Papadopoulos' Theory*

Papadopoulos [1984] suggested that the waves observed by *Murphy et al.* [1983] and *Shawhan et al.* [1984] evolve from a linear spectrum of lower hybrid waves driven by a beam of oxygen ions reflected from the space shuttle. The relevant instability is the modified-two-stream instability [*Krall and Liewer*, 1971]. No role is played in the theory by water "pickup" ions, and the nature of the required reflection process for the oxygen ions is not specified. Severe theoretical problems exist for efficient reflection of low-energy ions (ram energy of order 5 eV) off metallic or ceramic surfaces [e.g., *Hagstrum*, 1961; *Meyer et al.*, 1985; J. E. Borovsky, personal communication, 1989]. The majority of such ions are reflected as neutrals, and the ion reflection yield (and corresponding relative beam density) is almost invariably much less than 1%. In contrast, the theory developed in this paper involves Doppler-shifted lower hybrid waves driven by beam distributions of water pickup ions via the modified-two-stream instability. The primary difference between these two theories is the source and nature of the ion beam driving the lower hybrid waves. The pickup water ions naturally have relative number densities $\geq$10–20% in the near vicinity of the shuttle, as observed [*Grebowsky et al.*, 1987] and predicted theoretically [*Cairns*, 1990]. Accordingly, these much higher beam densities ($\geq$10–20% compared with $<$1%) imply much higher growth rates for waves generated by the water ion theory than for the reflection theory. This greatly favors the water ion theory developed here over *Papadopoulos*' [1984] theory. We conclude that Papadopoulos' theory is not viable unless oxygen ion reflection yields greater than 10–20% can be experimentally demonstrated for the space shuttle in an orbit similar to that for the Spacelab 2 and OSS 1 missions.

6. A New Theory for the Near-Zone Waves

In this section we develop a linear theory capable of explaining generation of waves with the general characteristics of the near-zone waves. This theory involves the generation of Doppler-shifted lower hybrid waves driven by beamlike distributions of water ions [*Cairns*, 1990] via the modified-two-stream instability [*Krall and Liewer*, 1971; *Papadopoulos*, 1984] in the near vicinity of the space shuttle. These water ions are produced by charge exchange between ionospheric oxygen ions and water molecules outgassed from the space shuttle. Use of water "pickup" ions as the source of instability is the principal difference between our theory and that of *Papadopoulos* [1984]; as argued in the last section, Papadopoulos' theory is not a viable explanation for the observed waves. A linear theory for the characteristics of the waves is then developed and discussed. This new theory is shown to explain most of the characteristics of the observed waves. The roles of spatial inhomogeneity and nonlinear effects in producing the observed wave spectrum are then discussed. Preliminary simulation results providing some support for inhomogeneity and nonlinear effects being important are summarized. The section ends with comments on the generation of waves at frequencies above several times the lower hybrid frequency.

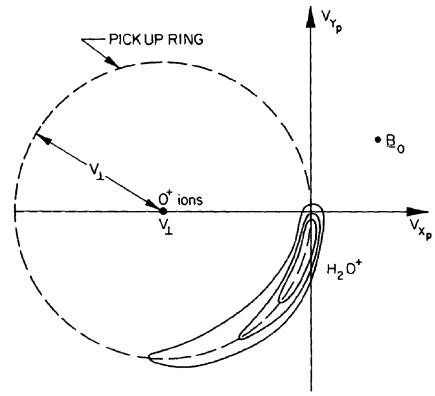

Fig. 8. Illustration of a "beam arc" distribution function of water ions in the V_{X_p}-V_{Y_p} phase space. Water ions have a gyrocenter drift $(-V_\perp, 0, 0)$ and gyrospeed of order $V_\perp$. Particle gyromotion corresponds to movement along the "pickup" ring in the clockwise direction.

6.1. *Linear Theory: Doppler-Shifted Lower Hybrid Waves*

Water ions are produced in the vicinity of the space shuttle by charge exchange between ionospheric oxygen ions and water molecules outgassed from the space shuttle [*Paterson and Frank*, 1989; *Cairns*, 1990]. *Cairns* [1990] has considered the distribution function of the pickup water ions and shown that a transition between a ringlike distribution function and a beamlike distribution function occurs with decreasing distance upstream from the space shuttle. In addition, the water ions increase monotonically in number density with decreasing distance upstream from the shuttle [*Cairns*, 1990]: within 10 m of the shuttle the water ions are observed [*Grebowsky et al.*, 1987] and expected theoretically to comprise in excess of 10% of the plasma ions. Within about 30 m from the shuttle (but not in the wake region) the water ion distributions are best described as "beam arc" distributions, corresponding to the water ions being found primarily in a finite section near zero velocity (relative to the shuttle) of a ring. Figure 8 shows these distribution functions in the X_P-Y_P-Z_p "pickup" coordinate system. Reviews of the pickup ion motions are given in the papers by *Paterson and Frank* [1989], *Cairns* [1990], and *Cairns and Gurnett* [1991]. Briefly, however, the water ions are born in a thermal distribution centered at zero velocity relative to the shuttle but experience a convection electric field due to the ionospheric plasma's motion across the magnetic field. The water ions then move with cycloidal orbits in the X_P-Y_P plane composed of a gyrocenter drift $(-V_\perp, 0, 0)$ and gyrospeed of order $V_\perp$ (modified by the initial thermal velocity of the ion) and thermal motions along the magnetic field. In contrast, the ionospheric plasma moves with velocity $(-V_\perp, 0, -V_\parallel)$ in this frame.

Within 30 m from the shuttle it appears appropriate to initially model the pickup water ions in terms of a Maxwellian beam distribution centered at zero velocity while the

ionospheric plasma drifts relatively (the influence of the ring component is discussed briefly below). We work in the pickup coordinate system, in which case the calculated wave frequencies are directly comparable with the observed wave frequencies. For now we restrict our attention to the case in which the orbiter moves exactly perpendicular to the magnetic field and $V_\parallel = 0$. The electrostatic dispersion equation is then

$$1 + \frac{\omega_{pe}^2}{k^2 V_e^2}\left(1 + \frac{\omega - k_x V_\perp}{2^{1/2} k_\parallel V_e} e^{-r_e^2} \sum_{m=-\infty}^{m=\infty} Z(y_{em}) I_m(r_e^2)\right)$$

$$+ \frac{\omega_{pO}^2}{k^2 V_O^2}\left(1 + \frac{\omega - k_x V_\perp}{2^{1/2} k_\parallel V_O} e^{-r_O^2} \sum_{m=-\infty}^{m=\infty} Z(y_{Om}) I_m(r_O^2)\right)$$

$$+ \frac{\omega_{pw}^2}{k^2 V_w^2}\left(1 + \frac{\omega}{2^{1/2} k V_w} Z(y_w)\right) = 0 \qquad (2)$$

In this equation the ionospheric electrons and oxygen ions are represented by magnetized Maxwellian distributions drifting with velocity $(-V_\perp, 0, 0)$ and have the standard forms for their contributions to the dispersion equation. The water ions are represented by an unmagnetized Maxwellian beam at zero velocity. Subscripts e, O, and w refer to the electrons, oxygen ions, and water ions, respectively. The functions J_m and I_m are Bessel functions of order m of the first and second kind, respectively. The arguments of these functions and the Fried-Conte function Z are $r_\alpha = k_\perp V_\alpha/\Omega_\alpha$ and $y_{\alpha m} = (\omega - k_x V_\perp - m\Omega_\alpha)/2^{1/2} k_\parallel V_\alpha$ for the electrons and oxygen ions, and $R_w = k_\perp V_\perp/\Omega_w$ and $y_w = \omega/2^{1/2} k_\perp V_w$ for the water ions. Standard definitions apply to the angular plasma frequencies $\omega_{p\alpha}$, gyrofrequencies Ω_α, number densities n_α, and thermal speeds V_α for species α.

The quantity $\omega - k_x V_\perp$ is the Doppler-shifted wave frequency seen by the ionospheric electrons and oxygen ions. A positive component k_x for a wave vector implies the wave vector is directed upstream along the X_P axis. When solving this equation we normalize all quantities relative to those for the oxygen ions. The standard normalization ratios used below are then $T_e/T_O = 2$, $T_w/T_O = 0.3$ ($T_O \sim 1000$ K), $V_\perp/V_O = 11$, and $\omega_{pO}/\Omega_O \sim 1000$ with an oxygen gyrofrequency $\Omega_O/2\pi$ of order 30 Hz. The nominal plasma parameters for the XPOP roll period are given in Table 1. All frequencies and growth rates calculated below are given in units of oxygen gyrofrequency. In these units the nominal lower hybrid frequency f_{LH}, given by the square root of the electron to oxygen mass ratio times the electron gyrofrequency, is 172 units.

Analytically, one expects this situation to give rise to Doppler-shifted lower hybrid waves via the so-called "modified-two-stream" instability [e.g., *Krall and Liewer*, 1971; *Papadopoulos*, 1984]. This may be seen as follows. The electron terms are treated by retaining only the $m = 0, \pm 1$ terms in the electron magnetization, expanding the modified Bessel functions in the limit $r_e^2 \ll 1$, retaining only first-order terms, and assuming that $k_\parallel \ll k_\perp$. The oxygen ions are treated by assuming that $\gamma \gg 1$ (in units of the oxygen gyrofrequency), so that the oxygen ions are effectively unmagnetized, and expanding the Fried-Conte function using the high phase speed expansion $(\omega/2^{1/2} k V_O \gg 1)$. The water ion contribution is expanded using the high phase speed approximation. Then, introducing the quantity δ defined by $\delta^2 = k_\parallel m_O/k^2 m_e n_O$, and assuming $(\omega - k_x V_\perp)^2 \ll \Omega_{se}^2$, equation (2) becomes

$$1 + \frac{\omega_{pe}^2}{\Omega_e^2} - \frac{\omega_{pO}^2(1+\delta^2)}{(\omega - k_x V_\perp)^2} - \frac{\omega_{pw}^2}{\omega^2} = 0. \qquad (3)$$

Rewriting this equation in terms of the (angular) lower hybrid frequency ω_{LH} and assuming $\omega_{pO}^2/\Omega_O^2 \gg 1$ leads to the dispersion equation

$$1 - \frac{n_O}{n_e}\frac{\omega_{LH}^2(1+\delta^2)}{(\omega - k_x V_\perp)^2} - \frac{n_w}{n_e}\frac{m_O}{m_w}\frac{\omega_{LH}^2}{\omega^2} = 0. \qquad (4)$$

Setting $\delta = 0$ and $m_w = m_O$, this equation is directly analogous to the dispersion equation for the usual two-stream instability in which Langmuir waves are generated by an electron beam and viewed in the reference frame of the beam [e.g., *Cairns*, 1989]. Accordingly [*Cairns*, 1989], for beams which satisfy the condition $n_w/n_e > 2.5(V_w/V_\perp)^3$ ($\sim 10^{-3}$ here), this equation predicts generation of strongly growing waves with dispersion relation $\omega_{rest} \sim k_x V_\perp$, frequencies near the lower hybrid frequency in the ionospheric plasma rest frame, and relatively small wave frequencies in the shuttle's rest frame. Finite values of δ, corresponding to the waves not propagating exactly perpendicular to the magnetic field, introduce no qualitative differences to this picture save that the maximum growth rate occurs for $\delta \sim 1$ (rather than $\delta = 0$) for the modified-two-stream instability.

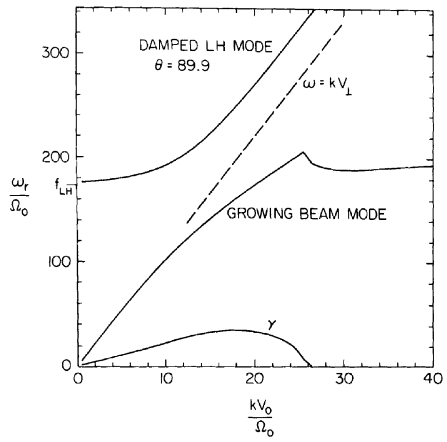

Fig. 9. Dispersion diagram for a water ion beam with $n_w/n_e = 0.05$, $V_\parallel = 0$, other plasma parameters as given in the text, and waves with wave vectors defined by $\theta = 89.9°$ and $\phi = 0°$. The damped lower hybrid mode and growing beam mode waves are shown. This figure is strongly reminiscent of the ordinary beam instability for growth of Langmuir waves.

Figure 9 shows the wave dispersion relation and growth rate in the ionospheric plasma frame for waves propagating along the X_P direction with an angle $\theta = 89.9°$ between the wave vector and the magnetic field direction (the Z_P axis). The relative water ion number density, n_w/n_e, is 5%. The dashed line shows the dispersion relation $\omega_{rest} = k_x V_\perp$ for comparison. A strong resemblance to the ordinary beam instability for Langmuir waves is apparent [e.g., *Cairns*, 1989, Figure 1]. Four important results may be inferred from

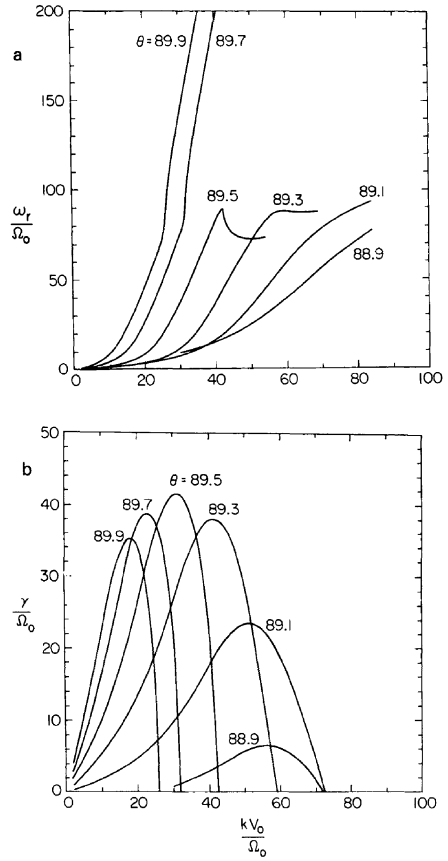

Fig. 10. (*a*) Observable wave frequencies (magnitudes) as a function of wavenumber for various angles θ (but $\phi = 0°$) and the plasma parameters of Figure 9. (*b*) Growth rates as a function of wavenumber for various angles θ. The waves are flutelike mode waves tightly restricted to perpendicular propagation, and the (observable) wave frequency increases with wavenumber.

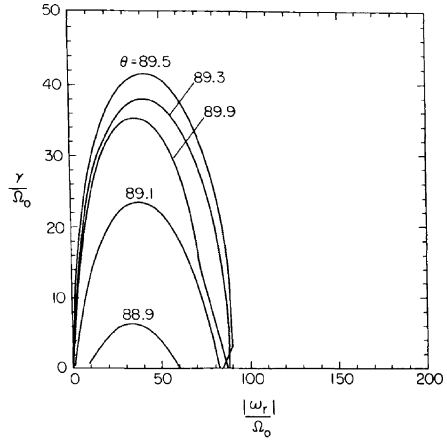

Fig. 11. Growth rates versus (observable) wave frequencies as a function of angle θ (with $\phi = 0°$) for the same plasma parameters as Figure 9. Maximum growth rates occur near $0.25 f_{LH}$.

this figure: (1) These waves are essentially beam-driven waves with $\omega_{rest} \sim k_x V_\perp$. (2) The waves have strong growth rates. (3) Since $\omega_r < k_x V_\perp$ for all wavenumbers k_x, these waves will be Doppler-shifted to low and negative frequencies (only the magnitude of the frequency is directly observable, however). (4) The higher-wavenumber waves will be Doppler-shifted to larger observable wave frequencies than the smaller-wavenumber waves.

Figures 10*a* and 10*b* present the dispersion relations and growth rate curves, respectively, for the waves in the PDP (or shuttle) frame for propagation at various polar angles θ between the magnetic field and the wave vector (and fixed propagation angle $\phi = 0°$) in the X_P-Y_P plane. The angle ϕ is defined by $k_x = k_\perp \cos \phi$. Figure 10*a* explicitly shows results 3 and 4 above; note that the fastest growing waves always occur on portions of the dispersion curve where the higher-wavenumber waves have higher frequencies. This is consistent with the interpretation in section 3 of the null patterns in the orbiter's plasma wake. The growing waves are clearly confined to angles $\theta > 88.8°$, with maximum growth occurring near $\theta \sim 89.6°$. Thus the waves are flutelike modes (with wave vectors almost perpendicular to the magnetic field), as expected for lower hybrid–like waves. The waves are unstable over a range of wavenumbers from 0 to 70 Ω_O/V_O. In comparison, a wavenumber of $30\Omega_O/V_O$ corresponds to a wavelength of 0.8 m for the nominal ionospheric parameters defined above. Electric fields with these wavelengths are observable using the PDP's double-sphere antenna.

Figure 11 compares curves of the growth rate versus frequency of waves with wave vectors directed at various angles θ and a fixed angle $\phi = 0°$ for the same plasma parameters as Figure 9. The frequency range over which growth occurs shows little variation with angle θ. Maximum growth is centered on a frequency of order $0.25 f_{LH}$; growth should occur over the frequency range from zero frequency to about $0.5 f_{LH}$. Variations in the angle ϕ for fixed θ show more effects. Figure 12 shows curves relating the wave frequency and growth rate for wave vectors directed at various angles ϕ and fixed $\theta = 89.5°$ for the same plasma parameters as Figure 9. The fastest growing waves remain concentrated near a frequency of order $0.25 f_{LH}$ while the

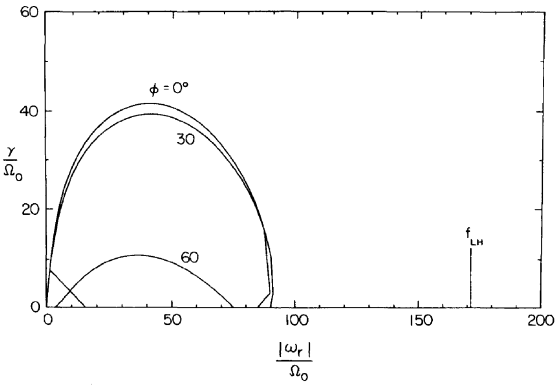

Fig. 12. Growth rates versus (observable) wave frequency as a function of angle ϕ and fixed angle $\theta = 89.5°$ for the plasma parameters in Figure 9. Growth is restricted to angles $\phi < 66°$.

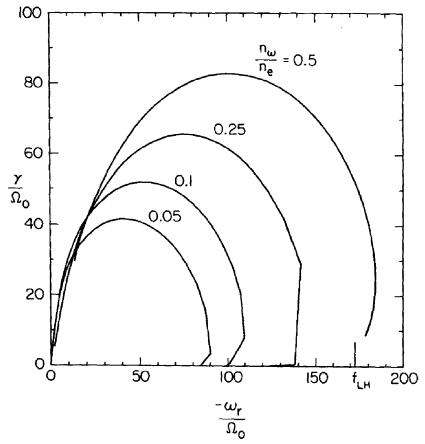

Fig. 13. Growth rates versus (observable) wave frequency as a function of beam density n_w/n_e for angle $\phi = 0°$ and angles θ with the maximum growth rate. Increasing the beam density increases the maximum growth rate, the frequency at which maximum growth occurs, and the extent of the growing waves in frequency, wavenumber, and wave vector directions.

bandwidth of growing waves decreases with increasing ϕ. However, the growth rates for the waves decrease rapidly with ϕ once $\phi > 50°$ and the waves are damped for $\phi > 66°$. As ϕ increases from zero, the wavenumbers $k_\perp$ of the fastest growing waves increase, so as to permit the resonance condition $\omega_{rest} \sim \Omega_{LH} \sim k_\perp \cos(\phi) V_\perp$ to be satisfied.

Lastly, we show in Figure 13 the effect of increasing the relative water ion number density n_w/n_e on the wave frequency at which the growth rate is maximum. Increasing the water ion number density increases both the center frequency and the bandwidth of the growing waves. Accordingly, linear theory predicts that the spatial gradient in water ion number density near the shuttle [*Cairns*, 1990] (when not in the wake region) implies an increase in the center frequency, bandwidth, and growth rate of the unstable waves with decreasing distance from the shuttle. The linear theory can therefore explain wave growth from near zero frequency up to a frequency of order f_{LH}.

6.2. *Discussion of the Linear Theory: A Role for Inhomogeneity and Nonlinear Effects*

The linear theory described above is capable of explaining the generation of waves (1) with large growth rates in the observed frequency range and range of observable wavenumbers, (2) with wave vectors essentially perpendicular to the magnetic field, as required by the free-flight observations, and (3) with wavenumber increasing with frequency, as required by the high-frequency wave nulls during wake transits. Unusual species temperatures, densities, or preheating of the electrons are not required. Indeed, higher electron temperatures should tend to damp the waves and reduce their angular range. The linear theory permits two qualitative explanations for the $V_\parallel/V_T$ effect described in section 2. First, as argued by *Cairns and Gurnett* [1991], the different motions of the pickup ions driving the waves and the ionospheric plasma convecting the waves imply that the waves will have minimum (maximum) growth lengths when $|V_\parallel/V_T|$ is large (small), thereby explaining the differences in amplitude. Second, by analogy with the ordinary two-stream instability [e.g., *Gary*, 1985], large values of $|V_\parallel/V_T|$ imply small effective beam speeds driving the waves, and eventually zero growth rates once below some threshold speed. This mechanism is illustrated in Figure 9 of *Cairns and Gurnett*'s [1991] paper. Extension of the linear theory to the general case $V_\parallel \neq 0$ is required before further development of these qualitative ideas. However, both mechanisms are qualitatively consistent with the observed waves being driven by water pickup ions, and so with the linear theory developed here.

The above points show that the linear theory predicts waves in very good agreement with the observed characteristics of the intense near-zone waves in the frequency range 0–f_{LH}. However, the linear theory is not capable of explaining the details of the frequency spectrum for the intense near-zone waves or the generation of the weak near-zone waves above f_{LH}. In particular, the linear theory predicts growth between zero frequency and about the lower hybrid frequency with a peak (corresponding to the maximum growth rate) in the range 0.25–0.75 f_{LH} depending on the relative number density of water ions (Figure 13). The observed waves cover this entire frequency range, thereby being qualitatively consistent with the linear theory. However, the maximum wave levels are theoretically predicted to be in the range 1.5–7.5 kHz (4 kHz $\leq f_{LH} \leq$ 9 kHz), well above the observed low-frequency peak at about 178 Hz and well below the observed peak near the lower hybrid frequency. This quantitative difficulty in explaining the details of the observed frequency spectrum should be expected for at least three reasons: (1) the limitations of the linear theory, (2) the neglect of inhomogeneity effects in the strongly inhomogeneous shuttle environment, and (3) the neglect of nonlinear effects which are often vital in determining the wave spectrum.

Improvements to the linear theory can be expected in a number of ways. A more exact representation of a beam arc distribution might involve superposing a beam distribution onto a lower-level ring distribution and considering both components in the linear theory. *Cairns and Gurnett* [1991] have considered generation of Doppler-shifted lower hybrid waves by a ring distribution. They find that growth is likely to be most effective near zero frequency, although wave growth up to frequencies of order $2f_{LH}$ is possible. Thus, considering the contribution of the ring component to the water ion distribution function might lead to a second peak in the growth rate at low frequencies, thereby leading to an explanation for the observed peak near 178 Hz for the near-zone waves. In addition, waves driven by ring distributions well away from the immediate vicinity of the shuttle [*Cairns and Gurnett*, 1991] and convecting into the near-zone region might explain some of the low-frequency near-zone waves. However, the free-flight data generally show low wave levels upstream from the shuttle. Further improvements to the linear theory could be made by including the effects of charge exchange and neutral-ion collisions to the linear dispersion equation. However, test solutions including these effects show little change from the corresponding solutions of equation (2). Therefore, in this paper, although we recognize that potential exists for modifying the linear theory to better explain the observational data, we defer further examination of the linear theory to future work on

the grounds that inhomogeneity effects and nonlinear effects are greatly more favored means to produce the details of the observed wave spectrum.

Inhomogeneity effects may be expected to limit effective linear growth of the waves (i.e., the wave vector for a wave with frequency ω must change with position for linear theory to predict further growth) and cause evolution of the wave spectrum away from the predictions of linear theory. Figure 13 demonstrates the significant changes in wave frequency and growth rate that should accompany the increasing water ion number density expected near the space shuttle [*Cairns*, 1990]. Thus convection of growing waves through the spatially inhomogeneous shuttle environment is likely to strongly modify the wave spectrum from the predictions of linear theory. We note that spatial inhomogeneity is also important in limiting the growth length of the waves in the first interpretation for the $V_\parallel/V_T$ effect given above and in the *Cairns and Gurnett* [1991] paper. Spatial inhomogeneity can also couple drift modes to sources of free energy [e.g., *Simons et al.*, 1980; *Pickett et al.*, 1989]. Thus, as suggested by *Pickett et al.* [1989] in another, related context, a drift mode instability coupling to the source of free energy in the water ion beam near the shuttle may provide an explanation for the low-frequency peak near 178 Hz in the near-zone waves. This suggestion will be pursued elsewhere.

Nonlinear processes involving lower hybrid waves, such as scattering off thermal ions, decay processes involving ion acoustic waves, modulational instabilities, and strong turbulence processes, have been discussed in the literature [e.g., *Musher et al.*, 1986]. The reasons for considering nonlinear processes in the present context are (1) modification of the wave spectrum predicted by linear theory and (2) production of new waves and associated peaks in the wave spectrum. Detailed discussions of these possibilities are not appropriate here; our purpose is merely to show that nonlinear processes may plausibly be important in determining the observed wave spectrum. The ratio of wave electric field energy to thermal plasma energy is of order 10^{-5} (for $n_e = 10^{11}$ m^{-3}) while the ratio of the total water ion kinetic energy to the thermal plasma energy is of order 5 for $n_w/n_e = 0.1$. Moreover, we point out that the linear theory predicts growth at wavelengths generally smaller than the effective antenna length during the XPOP roll (1.15 m) and free-flight mission (3.89 m). It is therefore probable that the high wave levels seen (total average broadband field of order 50 mV/m) are smaller than the actual wave levels in the plasma. These wave levels are considerable and imply that nonlinear processes, including strong turbulence processes, warrant considerable attention. Further support for consideration of nonlinear effects comes by comparing the time scales for growth and convection of the waves. For waves with a linear growth rate of $50\Omega_O$ typical in Figure 13, 10 e-folding growth periods correspond to a time of 10^{-3} s. During this time period a wave packet would be convected a maximum distance of 8 m (given the shuttle's orbital speed of 7.8 km s^{-1}) while a wave electric field would increase by a factor of 2×10^4. This distance is small compared with the expected extent of the region near the shuttle with beam distributions of water ions (~30 m [*Cairns*, 1990]) and comparable in size with the expected scale length of the gradient in the neutral water number density within 10 m of the space shuttle.

Nonlinear processes appear to be occurring in simulations relevant to the shuttle problem which we have performed in collaboration with G. Lu and C. K. Goertz. The two-dimensional electrostatic code used, the code PANIC [*Machida and Goertz*, 1988], incorporates a time-varying and spatially varying rate of charge exchange, consistent with collisional charge exchange between ionospheric oxygen and a spherical water gas cloud whose number density varies inversely with radial distance squared. This code is therefore suitable for studying the long time scale behavior of waves near the shuttle. Preliminary simulations runs show an initial growth phase of low-frequency waves (relative to the lower hybrid frequency), followed by a later phase in which the wave spectrum splits into two components, one near zero frequency and one near the lower hybrid frequency. These simulations therefore appear to produce a two-peaked frequency spectrum similar to the observed wave spectrum. Further work is required to see whether this agreement is fortuitous and to investigate the physics of these processes.

6.3. *Waves Observed Above Several Times the Lower Hybrid Frequency*

The wave data indicate that the broadband near-zone waves extend up to frequencies of order 50 kHz, corresponding to 5–10 times the lower hybrid frequency. The wave spectrum above the lower hybrid frequency shows only a smooth decrease without apparent structure. Linear theory for Doppler-shifted lower hybrid waves driven by a ring distribution of water ions [*Cairns and Gurnett*, 1991] can explain wave frequencies up to about 2 times the lower hybrid frequency. Similarly, the beam-driven Doppler-shifted lower hybrid waves considered in this paper are restricted (by the linear theory) to frequencies below the lower hybrid frequency. Therefore linear theories involving ring or beam distributions of water ions appear incapable of explaining the weak observed waves above about $2f_{LH}$. We note that *Hwang et al.*'s [1987] theory predicts growth above the lower hybrid frequency. However, Hwang et al.'s waves do not have wave vectors perpendicular to the magnetic field as implied by the free-flight data in section 4 even for wave frequencies well above $2f_{LH}$. Combining this point with the problems identified in section 5.1 for Hwang et al.'s theory, it appears that Hwang et al.'s theory is not a viable explanation for the observed waves above a few times the lower hybrid frequency. Investigations into nonlinear effects and mechanisms involving spatial inhomogeneity appear promising directions for further research into the origin of these high-frequency waves.

7. IMPLICATIONS OF THE $V_\parallel/V_T$ EFFECT FOR SHUTTLE MISSIONS

Detailed observations of plasma waves constitute an important diagnostic for active space experiments and investigations into the natural ionosphere. The data presented in this paper show that the intense broadband waves in the immediate vicinity of the space shuttle have total average electric fields of order 50 mV/m in the frequency range from 30 Hz to 10 kHz (the lower hybrid frequency). Removing this high, and probably dominating, background of waves should therefore be an important consideration in designing shuttle missions and orbiting facilities, such as the proposed space

station, intended as bases for research involving plasma waves. The dramatic $V_\parallel/V_T$ effect observed for the near-zone waves (Plate 1) offers a means to minimize the levels of orbiter-associated waves, as pointed out previously by *Cairns and Gurnett* [1991] for waves observed during the free-flight portion of the Spacelab 2 mission. In particular, the orbit of the platform should be designed so that $|V_\parallel/V_T|$ is close to 1 for as much of the orbit as possible. Plate 1*b* indicates that a minimum value $|V_\parallel/V_T| = 0.7$ should be chosen at this orbital height. These orbits are highly inclined with respect to Earth's equatorial plane. However, due to orbital constraints, present-day launching sites, and political realities, another approach is likely to be more attainable [e.g., *Cairns and Gurnett*, 1991]: the observing instruments and experiment package should be placed at a sufficient distance upstream from the shuttle or other outgassing facility to be outside the water/outgas cloud. Data from the PDP free-flight mission suggest that distances of order 1 km are appropriate [*Paterson and Frank*, 1989].

Nevertheless, further research into the origin and usefulness of the observed $V_\parallel/V_T$ effect is advisable. Explanations for the offsets between the centers of the wave nulls and the peaks in $V_\parallel/V_T$ should be pursued. Furthermore, as pointed out by *Cairns and Gurnett* [1991], an upper limit on $|V_\parallel/V_T|$ may exist due to driving of ion acoustic–like wave instabilities by the parallel drift between the water pickup ions and the ionospheric plasma. These instabilities are expected to be strongly temperature-dependent, implying possible variations with height and time of day in the ionosphere. Further work is required to investigate this possibility.

8. Conclusions

This paper contains a detailed observational characterization of the plasma waves observed within about 10 m of the space shuttle during the XPOP roll period of the Spacelab 2 mission. The frequency distribution of wave electric fields is best interpreted in terms of three components. The first, and primary, component is a uniform high level of waves covering the frequency range from 31 Hz to 10 kHz with only minor variations in amplitude with frequency. Two superposed peaks in this frequency range mark the two other components, and the wave levels decrease rapidly with increasing frequency above 10 kHz. The two superposed components have electric fields of order twice the steady level. The second component is defined by the low-frequency peak in the range 100–178 Hz. This low-frequency component merges smoothly back into the steady level of waves. The third component is found near the lower hybrid frequency. The spectral density and electric field amplitude of this component follow both the magnitude and the trend of the theoretical lower hybrid frequency. Wave power is observed consistently out to frequencies of order 56 kHz. No evidence is found for a high-frequency component localized above about 10 kHz due to the smooth falloff in the spectral density and integrated electric field profiles seen at these frequencies. The waves show a pronounced amplitude and frequency variation with the quantity $V_\parallel/V_T$ which measures the angle between the ionospheric magnetic field and the shuttle's velocity vector. Very low wave levels and small frequency extents are observed when $V_\parallel/V_T$ is near its maximum value, i.e., the shuttle is moving as close to parallel to the magnetic field as possible, and the highest wave levels and extents in frequency are observed when $V_\parallel/V_T$ is near zero. This implies that the waves are plausibly driven by water pickup ions [e.g., *Cairns and Gurnett*, 1991]. Strong analogies with the spectral characteristics (two peaks, one at the lower hybrid frequency and one near zero frequency) and the $V_\parallel/V_T$ effect observed during the free-flight portion of Spacelab 2 provide further hints that the near-zone waves are driven by pickup water ions. Observations of the waves below about 20 kHz during the free-flight mission imply that the near-zone waves have wave vectors oriented perpendicular to the magnetic field. The observation of nulls in the wave data which occur first at higher frequencies as the PDP spacecraft enters the density hole in the orbiter's wake implies that the higher-frequency waves have higher wavenumbers (shorter wavelengths) than the lower-frequency waves. Lastly, the observed near-zone waves have a total measured average broadband (frequency-integrated) electric field of order 50 mV/m. This field strength implies a ratio of electric field density to thermal plasma energy density of order 10^{-5}. Together with the prediction from linear theory that waves should grow with linear wavelengths smaller than the antenna length, so that the true field strength in the plasma is underestimated, this wave level implies that nonlinear effects may be important in understanding the evolution of the waves.

Detailed theoretical work on the near-zone waves is also performed in the paper. Recently, *Hwang et al.* [1987] developed a theory for the near-zone waves involving ion acoustic and ion-ion acoustic instabilities driven by the secondary ion streams observed in the near vicinity of the shuttle [*Stone et al.*, 1983, 1986]. Here we showed that this theory is inconsistent with the frequency distribution and wave vector orientations of the observed waves. In addition, Hwang et al.'s instabilities are suppressed for more nominal beam and plasma temperatures. A new theory involving Doppler-shifted lower hybrid waves driven by beamlike distributions of water ions [*Cairns*, 1990] in the near vicinity of the space shuttle is proposed and developed using linear theory. The relevant instability is the modified-two-stream instability. This linear theory can explain generation of waves with (1) frequencies ranging from near zero frequency to the lower hybrid frequency, (2) wave vectors essentially perpendicular to the magnetic field, (3) wavenumbers increasing with wave frequency, and (4) wavelengths observable by the PDP antenna. In addition, the theory permits two qualitative explanations for the $V_\parallel/V_T$ effect. These properties are all consistent with the properties of the observed near-zone waves and provide strong support for this theory. However, the linear theory cannot explain the details of the observed frequency spectrum of the waves. In particular, the theory predict growth over the frequency range of the primary, uniform component of the waves, but with a peak growth rate in the range $0.25–0.75\,f_{LH}$ and no peaks at the frequencies of the two observed peaks (or components) in the wave spectrum at low frequencies 100–178 Hz and the lower hybrid frequency itself. The linear (beam) theory cannot explain the observed low-level waves above the lower hybrid frequency. Explanations for the differences between the linear theory and the observed wave spectrum are discussed in terms of refining the linear theory, the effects of the strongly spatially inhomogeneous near-zone environment, and nonlinear effects. Including the effect of the ring component on the beam arc distributions of water

ions in the near vicinity of the space shuttle [*Cairns*, 1990] should lead primarily to increased growth at low frequencies, as well as less favored growth up to frequencies near $2f_{LH}$ [*Cairns and Gurnett*, 1991]. Convection of the growing waves through the spatially inhomogeneous shuttle environment, and so the varying wavenumbers required for a wave of a given frequency to be linearly unstable, is expected to modify the frequency spectrum of growing waves. Furthermore, coupling of a drift mode associated with the density gradients to the free-energy source in the water ions might lead to an instability at low frequencies [e.g., *Simons et al.*, 1980; *Pickett et al.*, 1989], thereby perhaps explaining the component near 100–178 Hz. The high wave levels imply that nonlinear effects, such as decay processes involving ion acoustic waves, modulational instabilities, and strong turbulence processes [e.g., *Musher et al.*, 1986], may be very important in determining the frequency spectrum of the waves. Preliminary simulations of the shuttle environment run in collaboration with G. Lu and C. K. Goertz also indicate that nonlinear processes are important. In summary, while the linear theory developed here successfully explains many of the characteristics of the near-zone waves, further theoretical work involving the effects of wave nonlinearities and spatial inhomogeneity is required to explain the details of the observed wave frequency spectrum. Finally, we note that the $V_\parallel/V_T$ effect observed for the near-zone waves has similar implications for design of future shuttle missions to those described by *Cairns and Gurnett* [1991]: orbits for shuttle missions requiring minimal plasma wave backgrounds should be highly inclined to Earth's equatorial plane with $|V_\parallel/V_T| > 0.7$ over as much of the orbit as possible. Otherwise, these missions should be performed using free-flying spacecraft located at least 1 km upstream of any outgassing facility.

Acknowledgments. We acknowledge financial support the NASA grant NAGW-1488 from NASA Headquarters and NASA grant NAG3-449 from NASA Lewis Research Center. Helpful discussions with J. S. Pickett and W. S. Kurth concerning the Spacelab 2 mission are also gratefully acknowledged.

The Editor thanks Associate Editor D. Winske for handling the review process on this paper and D. Gallagher and another referee for their assistance in evaluating this paper.

REFERENCES

Cairns, I. H., Electrostatic wave generation above and below the plasma frequency by electron beams, *Phys. Fluids B*, *1*, 204, 1989.

Cairns, I. H., Transition from ring to beam arc distribution functions of water ions with distance upstream from the space shuttle orbiter, *J. Geophys. Res.*, *95*, 15,167, 1990.

Cairns, I. H., and D. A. Gurnett, Control of plasma waves associated with the space shuttle by the angle between the orbiter's velocity vector and the magnetic field, *J. Geophys. Res.*, *96*, 7591, 1991.

Farrell, W. M., D. A. Gurnett, and C. K. Goertz, Coherent Cerenkov radiation from the Spacelab 2 electron beam, *J. Geophys. Res.*, *94*, 443, 1989.

Gary, S. P., Electrostatic instabilities in plasmas with two electron components, *J. Geophys. Res.*, *90*, 8213, 1985.

Gary, S. P., and N. Omidi, The ion-ion acoustic instability, *J. Plasma Phys.*, *37*, 45, 1987.

Grebowsky, J. M., H. A. Taylor, Jr., M. W. Pharro III, and N. Reese, Thermal ion perturbations observed in the vicinity of the space shuttle, *Planet. Space Sci.*, *35*, 501, 1987.

Gurnett, D. A., W. S. Kurth, J. T. Steinberg, and S. D. Shawhan, Plasma wave turbulence around the shuttle: Results from the Spacelab-2 flight, *Geophys. Res. Lett.*, *15*, 760, 1988.

Hagstrum, H. D., Reflection of noble gas ions at solid surfaces, *Phys. Rev.*, *123*, 758, 1961.

Hwang, K. S., N. H. Stone, K. H. Wright, Jr., and U. Samir, The emissions of broadband electrostatic noise in the near vicinity of the shuttle orbiter, *Planet. Space Sci.*, *35*, 1373, 1987.

Krall, N. A., and P. C. Liewer, Low-frequency instabilities in magnetic pulses, *Phys. Rev. A*, *4*, 2094, 1971.

Machida, S., and C. K. Goertz, The electromagnetic effect on the critical ionization velocity process, *J. Geophys. Res.*, *93*, 11,495, 1988.

Meyer, O., G. Linker, and F. Kappeler (Eds.), *Ion Beam Surface Layer Analysis*, Plenum, New York, 1985.

Murphy, G. B., S. D. Shawhan, L. A. Frank, N. D'Angelo, D. A. Gurnett, J. M. Grebowsky, D. L. Reasoner, and N. Stone, Interaction of the space shuttle orbiter with the ionospheric plasma, Spacecraft/Plasma Interactions and Their Influence on Field and Particle Measurements, *Eur. Space Agency Spec. Publ., ESA SP-198*, 73, 1983.

Musher, S. L., A. M. Rubenchik, and I. Ya. Shapiro, Nonlinear effects in the propagation of an ion beam across a magnetic field, *Sov. Phys. JETP*, Engl. Transl., *63*, 519, 1986.

Omidi, N., Broadband electrostatic noise produced by ion beams in the Earth's magnetotail, *J. Geophys. Res.*, *90*, 12,330, 1985.

Papadopoulos, K. D., On the shuttle glow (the plasma alternative), *Radio Sci.*, *19*, 571, 1984.

Paterson, W. R., and L. A. Frank, Hot ion plasmas from the cloud of neutral gases surrounding the space shuttle, *J. Geophys. Res.*, *94*, 3721, 1989.

Pickett, J. S., N. D'Angelo, and W. S. Kurth, Plasma density fluctuations observed during space shuttle orbiter water releases, *J. Geophys. Res.*, *94*, 12,081, 1989.

Reasoner, D. L., S. D. Shawhan, and G. Murphy, Plasma Diagnostics Package measurements of ionospheric ions and shuttle-induced perturbations, *J. Geophys. Res.*, *91*, 13,463, 1986.

Shawhan, S. D., Description of the Plasma Diagnostics Package (PDP) for the OSS-1 shuttle mission and JSC chamber test in conjunction with the fast pulse electron gun (FPEG), in *Artificial Particle Beams in Space Plasma Studies*, edited by B. Grandel, p. 419, Plenum, New York, 1982.

Shawhan, S. D., G. B. Murphy, and J. S. Pickett, Plasma Diagnostics Package initial assessment of the shuttle orbiter plasma environment, *J. Spacecr. Rockets*, *21*, 387, 1984.

Simons, D. J., M. B. Pongratz, and S. P. Gary, Prompt striations in ionospheric barium clouds due to a velocity space instability, *J. Geophys. Res.*, *85*, 671, 1980.

Stone, N. H., U. Samir, K. H. Wright, Jr., D. L. Reasoner, and S. D. Shawhan, Multiple ion streams in the near vicinity of the space shuttle, *Geophys. Res. Lett.*, *10*, 1215, 1983.

Stone, N. H., K. H. Wright, Jr., K. S. Hwang, U. Samir, G. B. Murphy, and S. D. Shawhan, Further observations of space shuttle plasma-electrodynamic effects from OSS-1/STS-3, *Geophys. Res. Lett.*, *13*, 217, 1986.

Tribble, A. C., J. S. Pickett, N. D'Angelo, and G. B. Murphy, Plasma density, temperature, and turbulence in the wake of the shuttle orbiter, *Planet. Space Sci.*, *37*, 1001, 1989.

I. H. Cairns and D. A. Gurnett, Department of Physics and Astronomy, University of Iowa, Iowa City, IA 52242.

(Received June 1, 1990;
revised January 17, 1991;
accepted March 4, 1991.)